Diffusional microfluidics for protein analysis

Huimin Xie[1], Yuanxi Yang[2], Chenghao Xia[1], Tung-Chun Lee[3], Qiaosheng Pu[1*], Yang Lan[2*], Yuewen Zhang[1*]

[1] College of Chemistry and Chemical Engineering, Lanzhou University, Lanzhou, Gansu 730000, P. R. China

[2] Centre for Nature Inspired Engineering, Department of Chemical Engineering, University College London, London, WC1E 7JE, United Kingdom

[3] Institute for Materials Discovery, University College London, London, WC1H 0AJ, United Kingdom

* Corresponding author. E-mail: puqs@lzu.edu.cn; yang.lan@ucl.ac.uk; zhangyw@lzu.edu.cn

Abstract

Wastewater-based epidemiology (WBE) is an emerging tool to monitor public health and the outbreak of infective diseases. It requires real-time information by measuring chemicals or biomarkers in wastewater generated by people at community-level for WBE analysis. Protein-based biomarkers provides valuable insights into community public health. However, due to the complexity of wastewater, the bottleneck of protein analysis in WBE lies in the lack of high-sensitive, cost-efficient and high-throughput analytical techniques. Diffusional microfluidics, which involves co-flowing streams of analytes and buffer under laminar flow conditions, allows the detection and analysis of biomolecules in their native state via the study of their diffusive behaviour in flow. In this review, recently developed analytical techniques, microfluidic diffusional sizing, free-flow electrophoresis, and hydrodynamic focusing microfluidic mixer, that are based on diffusional microfluidics are reviewed. Their applications in protein analysis including protein sizing, protein-protein interaction, protein separation and protein identification are highlighted.

Keywords: Diffusional microfluidics; Microfluidics; Protein analysis; Protein biomarker detection; Wastewater-based epidemiology

1. Introduction

Wastewater-based epidemiology (WBE) was firstly outlined as an analytical tool to investigate the illicit and misused drugs in local community by quantitatively or qualitatively analysing chemicals from wastewater [1]. Wastewater is also an ideal medium for pathogenic microorganisms such as viruses, bacteria, parasites, parasitic worms and protozoa [2-3]. Thus, by analysing pathogens and/or their biomarkers in wastewater at community-level, WBE is also developed to understand the health of local communities and serve as an early warning system for outbreaks of infective diseases [4-4]. For example, WBE has recently been used to monitor the COVID-19 outbreak; the RNA of SARS-CoV-2 was quantified in sewage to track the disease infection in local community [6-7]. Among the pathogens and biomarkers in wastewater, proteins have attracted increasing attention as 1) proteins are particularly useful biomarkers to track pathogenic microorganisms in wastewater as they are often the effectors of diseases [4], 2) proteomics in WBE can provide valuable new insights into community public health.

However, due to the complexity of wastewater, the bottleneck of protein analysis for WBE lies in the lack of high-sensitive, cost-efficient and high-throughput analytical techniques [3].

Microfluidics, which processes small amounts of fluids with channel dimensions of tens to hundreds of micrometres, provides a platform to develop analytical techniques that can potentially overcome these challenges [7]. For its applications in analysis, microfluidics offers a number of useful capabilities, including consuming small quantities of samples, rapid measurements on the order of tens of seconds, solution analysis in a confined environment, portable analytical device for potential on-site measurements, and high modularity to integrate other functionalities [8], which are all desirable features for protein analysis in WBE [9-11]. Based on the flow type, microfluidics can be classified as droplet-based microfluidics and continuous-flow microfluidics [8]. Droplet-based microfluidics contains a dispersed phase and a continuous phase to generate highly monodispersed microdroplets, which can be employed as miniaturised containers for potential high-throughput analysis [12]. For the applications of droplet-based microfluidics in WBE, we refer readers to ref. [13] for a detailed discussion on quantification of pathogen biomarkers, single-cell analysis, and living cell biosensing using droplet-based microfluidics. Continuous-flow microfluidics rely on a steady flow through the microchannels for fluid process which enables uninterrupted analysis of samples within a device [8]. Diffusional microfluidics is a subject of continuous-flow microfluidics which achieves fluid mixing or separation only through diffusion within a microfluidic device [14].

In this review, we aim to highlight recent advances in diffusional microfluidics and its application in protein analysis. The basis of diffusional microfluidics including its working conditions will be firstly introduced to provide the scientific background. Then, the classic device designs to fulfil diffusional microfluidics will be presented to briefly demonstrate the working principles of diffusional microfluidics. Follow by that, recently developed analytical techniques based on diffusional microfluidics and their application in protein analysis will be highlighted. At the end of this review, challenges and perspective of future application of diffusional microfluidics in WBE will be discussed after the conclusion.

2. The basis of diffusional microfluidics

In our day-to-day experience with fluids, random eddies continuously disturb fluid elements in bulk solution, which dramatically increase the rate of fluid mixing [8]. In microchannels of microfluidic device, however, fluid behaviour is dramatically different. Fluid flow at the microscale is normally in laminar which means each plane of fluid flows smoothly in parallel with each other [8,14-16]. The naturally arised laminar flow in the microchannels is resulted from the low inertial forces of fluid comparing to the viscous forces which can be characterised by Reynolds number (*Re*) [14-17]. *Re* is a

dimensionless parameter that defines fluid as being turbulent or laminar. It is calculated by the ratio of inertial to viscous forces.

$$Re = \frac{\rho v L}{\mu}$$

, where ρ is the density of fluid; v is the flow rate; L is the characteristic length, for microfluidic device it is given by the hydraulic diameter of the channel (typically span from 10 to 2000 μm) and μ is the dynamic viscosity of fluid. Laminar conditions occur when *Re* is smaller than 2300 [14-15,17]. For common microfluidic devices, the value of *Re* is typically smaller than 1 which ensures laminar flow within microfluidic devices [17-19]. With this prerequisite, fluid mixing within microfluidic device can only occur by diffusion as turbulent mixing is completed suppressed, which results in significantly longer mixing time than that in bulk solution. It also means that the concentration gradient of flow ingredients, created by purely diffusion within the laminar flow, would last much longer than in bulk solutions. In other words, temporal separation of flow ingredients can be achieved without the need of a solid boundary.

In addition, fluid properties in microfluidic device are greatly affected by the competition between convection and diffusion which can be characterised by Péclet number (*Pé*) [14,18-19]. *Pé* is a dimensionless parameter that can be calculated by the ratio of advective transport rate to diffusive transport rate.

$$P\acute{e} = \frac{Lv}{D}$$

, where L is the characteristic length; v is the linear flow velocity and D is the diffusion coefficient. When *Pé* is very large ($Pé > 10^7$), diffusion within a microfluidic device can be neglected because the advective transport of fluid is extraordinarily faster than diffusion [19]. At the other extreme, a small *Pé* ($Pé < 1$) indicates that the diffusion processes of fluid are dominant within the length scale of microfluidic device [19]. Fluid mixing, thus, happens only in a certain area through diffusion. In contrast, at an intermediate *Pé* value, the advective transport of fluid is faster than diffusive transport. Therefore, a rich amount of fluid mixing states can be observed along the downstream within the microchannels of a microfluidic device [18-19]. It also means that the diffusion process of ingredients within the fluid flow is location dependent. In other words, spatial separation of flow ingredients without a solid boundary is possible in a microfluidic device. Diffusional microfluidics works at an intermediate *Pé* value.

The possibility to achieve both temporal and spatial separation of ingredients in a diffusional microfluidic device enables the application of diffusional microfluidics in analytical sensing by extracting the physical information of analytes from their diffusive behaviour.

3. Classic design of diffusional microfluidic devices

One basic design to achieve diffusional microfluidics is the so-called T-sensor [20]. As shown in Fig. 1A, T-sensor has two inlets and one outlet, involving two fluid streams that enter the T-sensor separately and merge to flow adjacently through a microchannel (because of low *Re* at the microscale). Fluids, solutes, and suspended particles, thus, only mix through diffusion in the laminar flow, where small ingredients diffuse longer average distance per time than larger ingredients [20]. When it is operated at intermediate *Pé*, it forms an interdiffusion zone (sector) within the middle of the microchannel (Fig. 1A). The key parameters that control the interdiffusion zone are the ingredient diffusivity, channel length, width and flow rate [20]. The interdiffusion zone can be determined and measured by labelling with a fluorescent marker which gives information on analyte concentration, diffusivity, etc. T-sensor based diffusional microfluidic devices, thus, have been widely employed for chemical sensing [21-22].

Another basic design of diffusional microfluidics is the H-filter (Fig.1B). H-filter [23] is essentially similar to the T-sensor but has two outlets. Fluids, solutes and suspended particles within the combined stream diffuse differently, depended on their diffusion coefficient, flow rate, and dimensions of the mcirochannels (channel width, length and height). Basically, in the combined stream, small ingredients diffuse faster than the larger ones and will traverse the middle section of the channel onto the other side, while larger ingredients remain in the same side as they flow in (Fig. 1B). Therefore, ingredients separation can be achieved in the H-filter. While many other separation methods require a physical boundary, mechanical agitation, and/or external fields (electrical or gravitational) [23], it is not necessary for H-filter as it relies on purely diffusion which facilitates further biological analysis in their native state. In addition, H-filter enables the potential for direct analysis of complex samples without the need of prior purification which is a desirable feature for WBE.

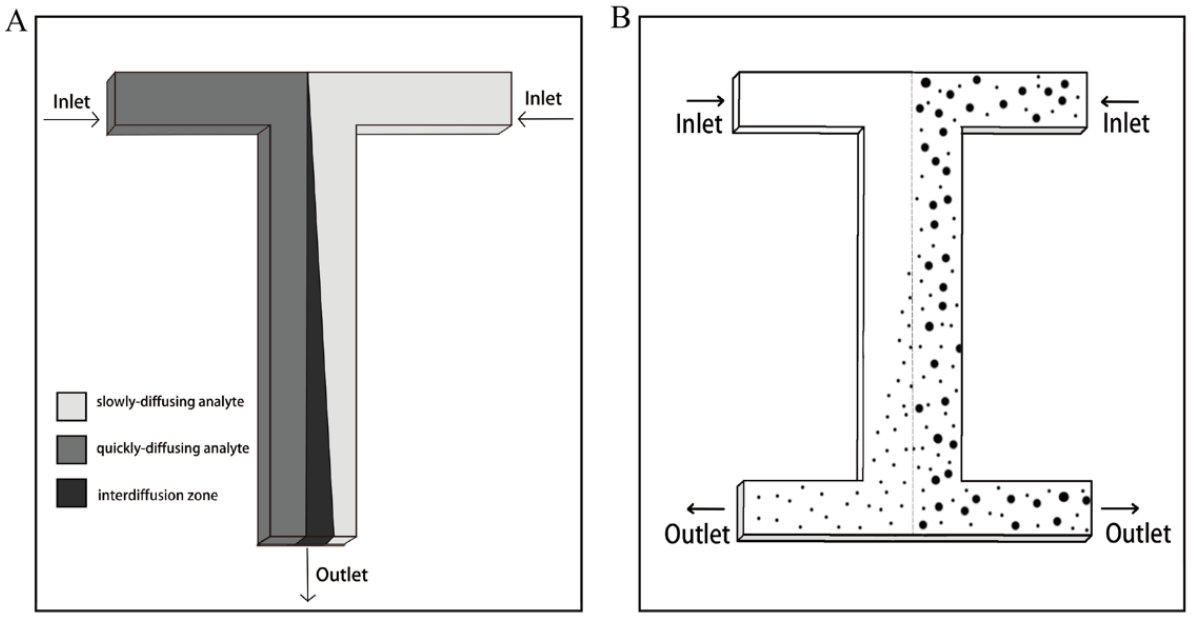

Fig. 1 (A) The schematic of T-sensor. Fluids are in laminar flow within the microchannels and mix only through diffusion. Small ingredients diffuse quicker than larger ingredients. (B) The schematic of H-filter. In the sample mixture, small ingredients diffuse faster than the larger ones and will traverse the middle section of the channel onto the other side, while larger ingredients remain in the same side as they flow in. Ingredients with different sizes can be separated using the H-filter.

4. Diffusional microfluidics-based protein analytical techniques

4.1 Microfluidic diffusional sizing (MDS)

Recently, a sizing technique based on diffusional microfluidics, named microfluidic diffusional sizing (MDS) [24], has been developed for protein analysis in terms of protein sizing [25-28], protein-protein interaction [25-31], protein separation [30] and protein identification [32-33]. In this technique, MDS devices are designed based on either the T-sensor or H-filter. The diffusion coefficient *D* of protein can be extracted from the mixing rate of proteins in the laminar flow by observing the time-evolution of the interdiffusion zone. The interdiffusion zone can be observed under a fluorescence microscope when proteins are either pre-labelled or post-labelled with a fluorescent dye. For protein that has large number of tryptophan and tyrosine, the interdiffusion zone can even be observed without any dye labelling because of its intrinsic fluorescence [34]. After obtaining the diffusion coefficient *D*, the average hydrodynamic radius (R_h) of the proteins can be calculated accordingly based on the Stokes-Einstein equation.

$$D = \frac{k_B T}{6\pi\eta R_h}$$

, where k_B is the the Boltzmann constant, T is temperature (K), η is the solution viscosity, D is the diffusion coefficient and R_h is the hydrodynamic radius.

MDS allows the measurement of average R_h without a bias towards large protein which is one of the major limitations of dynamic light scattering (DLS). Moreover, the measurements are performed in solution without interference from a solid boundary (as measurements using gel electrophoresis) which allows analysis of protein under their native states. In addition, by analysing the changes of protein R_h with or without the presence of interacting partners, protein interactions can be studied, and related binding affinity can be calculated.

Arosio *et al.* [25] designed a MDS device based on the T-sensor for protein analysis using dye-labelled proteins (Fig. 2A). In this design, the stream with dye-labelled proteins is sandwiched by two flanking buffer flows. And the proteins can laterally diffuse into the buffer streams under the laminar flow. The diffusion can be observed under fluorescent microscope as the proteins are pre-labelled with fluorescent dye. By measuring the width of the interdiffusion zone at certain locations of the microchannel (detection points) under fluorescence microscope, the diffusivity of proteins can be calculated (Fig. 2A detection region) and, consequently, the related R_h can be calculated based on the Stokes-Einstein equation. To ensure the protein stream precisely located in the centre of the channel, a multistage nozzle that is ten times wider than the diffusion channel is introduced. Besides**,** a high channel aspect ratio (1:12) has been considered to ensure an intermediate *Pé* number so that all protein particles explore the whole channel height within the MDS device. The MDS device has been validated by measuring the average sizes of proteins, peptides and even fluorescence labelled nanoparticles with the size range from 1 to 100 nm. The R_h measured by the MDS device are consistent with that measured by conventional techniques such as DLS. Compared with DLS, this MDS requires a significantly smaller amount of sample. The authors used the same MDS device to further detect protein-protein interactions [25]. The interactions between dye-labelled α-synuclein, a protein whose aggregation is related to the Parkinson's disease, and nanobody (NbSyn87), a single domain antibody fragment, have been conformed based on the increased R_h when the α-synuclein is titrated with NbSyn87 nanobody [25]. The authors further demonstrate the power of the MDS device for analysing mixtures of proteins via the deconvolution of experimental signals into the contributions that are from the individual protein (Fig. 2A (e)) [25]. Basically, the distribution of the diffusion coefficients ($\rho(D_i)$) of the species in solution is reflected from the shape of the concentration profile (c(x)) as a linear superposition. The distribution of $\rho(D_i)$ as a function of diffusion coefficients can be obtained via inverting the linear superposition relationship using a regularisation algorithm. A regularization coefficient (α), which is determined by calibration with known standards, is introduced to ensure stability in the presence of experimental noise. Global analysis of several diffusion profiles, thus, enables the deconvolution of experimental signal into a linear combination of simulated standard profiles, thereby leading to the evaluation of the size distribution of proteins in the mixture. The acquisition of a large number of

diffusion profiles is a key factor to assure the robustness of the method and allow clear resolution of individual size peaks of proteins in a mixture.

Using the same MDS device, Gang *et al*. [26] investigated the interaction between dye-labelled α-synuclein and negatively charged lipid vesicles which is not detectable using DLS. The R_h of α-synuclein is measured when the lipid vesicles are titrated (Fig. 2B). Thus, the dissociation constant and binding stoichiometry between α-synuclein and the vesicles can be characterized. Wright *et al*. [27] studied the self-assembly behaviour of chaperones (Hsp70) by monitoring the R_h change of dye-labelled SBD641(subdomain of HsP70) as a function of SBD641 concentration and time (Fig. 2C). Scheidt *et al*. [28] explored the function of chaperones towards the aggregation of dye-labelled amyloid-β (M1-42) peptide by following the size variation of amyloid-β (M1-42) fibrils with the presence of chaperone (either brichos domain or clusterin). The results show that clusterin chaperone can inhibit the elongation of amyloid-β fibrils (Fig. 2D). Scheidt *et al*. [28] also studied the interactions between the fibrils of α-synuclein and the small heat-shock protein αB-crystallin with the MDS device. By measuring the diffusion coefficient of bound and unbound chaperones, the thermodynamics and kinetics of binding can be studied within minutes.

Fiedler *et al*. [30] reported another MDS device, designed based on the H-filter, to study the neutralisation of SARS-CoV-2 (Fig. 2E), through the quantification of the interactions between the SARS-CoV-2 spike protein (S1) and the angiotensin-converting enzyme 2 (ACE2, which is virus receptor on the cell), as well as interactions between S1 and an antibody (NAbs). As shown in Fig. 2E, sample containing either mixture of dye-labelled ACE2 and S1, mixture of NAbs and dye-labelled S1, or mixture of dye-labelled ACE2, S1 and NAbs is loaded into the MDS device together with a flanking flow of buffer. Only the unbound proteins diffuse into the buffer stream as they are smaller than the protein complex. Consequently, the unbound proteins and protein complex are separated into two observation regions at the end of the diffusion chamber. The average R_h of the proteins in the sample is then determined by the ratio of fluorescence between the two observation regions, leading to the quantification of dissociation constants between either S1 and ACE2 or NAbs and S1. These results can be used to indicate the level of SARS-CoV-2 inhibition in human serum.

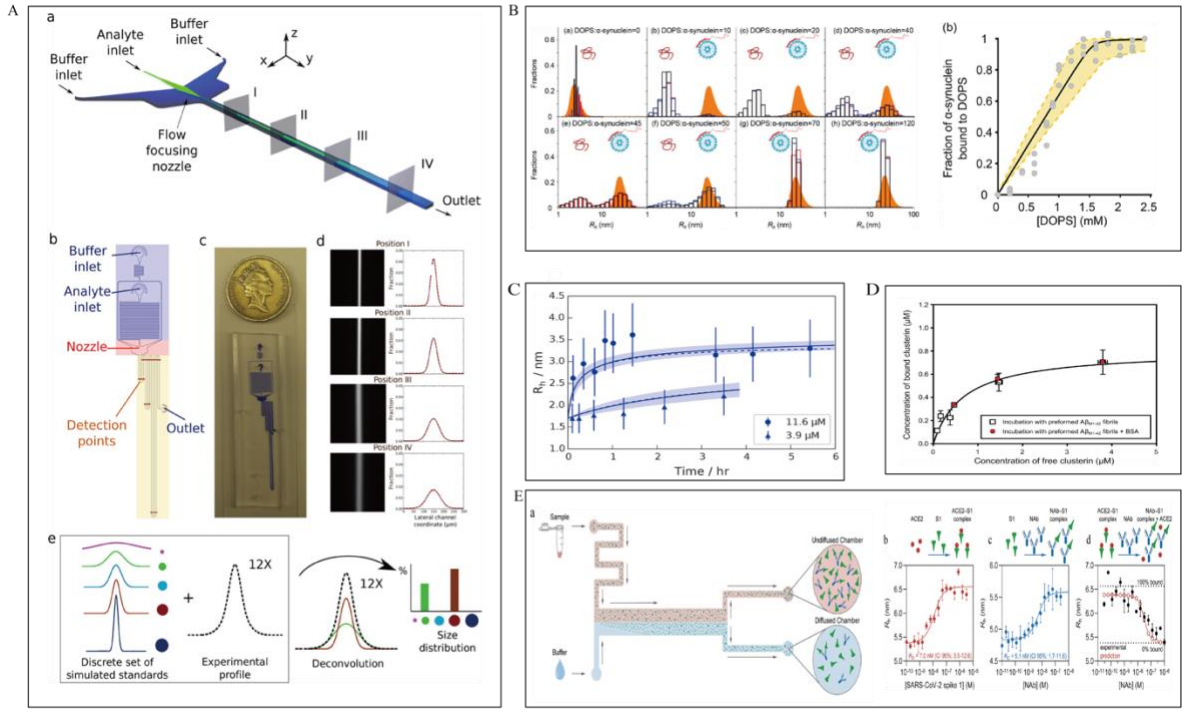

Fig. 2 (A) (a)-(c), The design of microfluidic diffusional sizing device. (d), Fluorescent images of colloid analytes at different positions along the microchannel and the comparison between measured and simulated diffusion profiles. (e), Global analysis of different diffusion profiles both in time and space to deconvolute the experimental signal into a linear combination of simulated standard profiles{Reprinted with permission from Ref. [25]}. (B) (a), Distribution profiles and R_h of α-synuclein measured by MDS (bars) and DLS (filled curves) in the absence and presence of vesicles. (b), Characterisation of the binding between α-synuclein and vesicles with MDS {Reprinted with permission from Ref. [26]}. (C) The R_h of SBD641 at different concentrations measured by MDS {Reprinted with permission from Ref. [27]}. (D) Binding curve of clusterin to amyloid-β (M1-42) fibrils measured by MDS {Reprinted with permission from Ref. [28]}. (E) (a), The neutralisation of SARS-CoV-2 is investigated using H-filter type MDS device. The R_h of analytes is calculated from the ratio of fluorescence intensities in the diffused chamber and the undiffused chamber. (b-d), The study of equilibrium binding of ACE2-S1, S1-NAb and NAb-S1 ACE2 complex within the MDS, respectively {Reprinted with permission from Ref. [30]}.

Fluorophore labelling are prone to affect the conformational structure of proteins, resulting in false biochemical properties of protein. Yates *et al.* [31] thus developed a MDS device for protein analysis under their native state using a latent protein labelling strategy (Fig. 3A). As shown in Fig. 3A, the protein and buffer stream with equal volumetric flow rates meet at the beginning of a diffusional channel (labelled t_0, Fig. 3A). At this point, the protein and buffer stream span half the width of the diffusional channel, separately. Subsequently, protein diffuse laterally into the buffer stream along with the flow direction in the diffusional channel. At the end of the diffusional channel (t_D), a third of the total stream is diverted into a latent labelling region where the diffused proteins are quantitatively labelled with a dye molecule of o-phthalaldehyde (OPA). Measuring the fluorescence intensity in the observation region defines the total concentration of protein diverted for labelling at position t_D, which in turn reveals the protein distribution at position t_D, allowing determination of R_h of protein by comparison with values simulated for particles of known R_h values. With this technique, R_h of biomolecules and heterogenous mixtures can be determined at attomole level. The high sensitivity of the MDS technique is desirable feature for the application of WBE. Moreover, the interaction between monomeric α-synuclein and a nanobody (NbSyn2) is studied under their native states based on the variation of R_h

values [31]. Using the same MDS device, Zhang *et al*. [35] investigated the stability of bovine serum albumin (BSA) under different pH conditions (Fig. 3B). Based on the measured average R_h and calculated linear interpolation, the fraction of folded BSA can be calculated. This method provides a new approach for studying the structural stability of proteins and other substances under native state of protein [35].

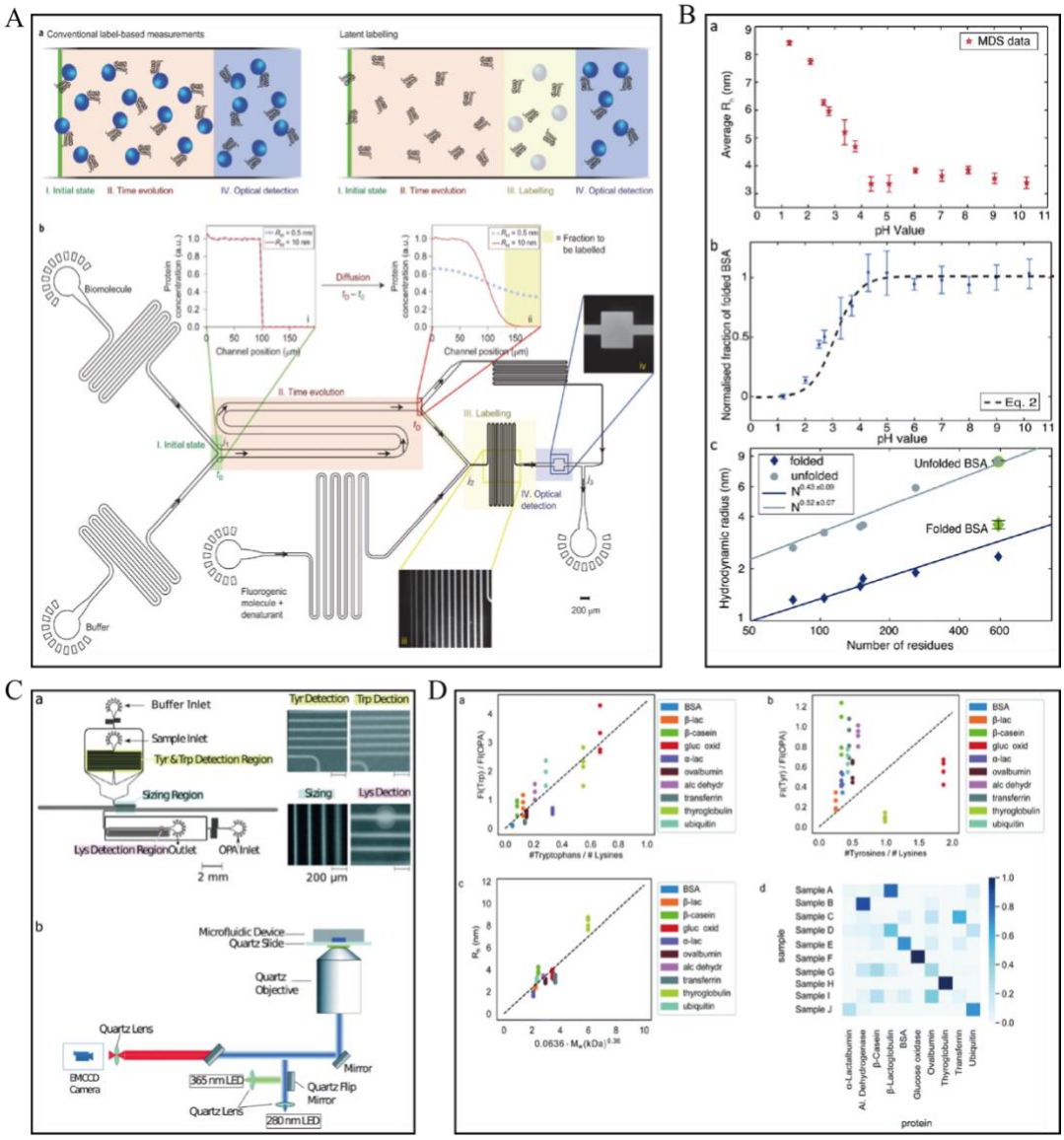

Fig. 3 (A) Latent labelling microfluidic diffusional sizing device {Reprinted with permission from Ref. [31]}. (B) (a), Average R_h of BSA measured with the latent labelling microfluidic diffusional sizing device under various pH conditions. (b), Normalized fraction of folded BSA derived from the measured R_h. (c), Fitted the measured folded and unfolded BSA to the literature value of average R_h versus the number of residues in a polypeptide chain {Reprinted with permission from Ref. [35]}. (C) The platform used for obtaining multidimensional signatures for proteins. (a), The MDS microfluidic device used for extracting a multidimensional characteristic signature of each analyte; (b), Schematic of the UV-LED fluorescence microscope {Reprinted with permission from Ref. [33]}. (D) Protein identification using the MDS device. (a)-(c), The ratio of the measured physical parameters. (d), The measured signals for each of the ten samples (A–J) were converted to estimates of their sequence-composition using the relationships outlined in panels (a)-(c) and the latter estimates were used to evaluate the probabilities of each of the ten samples being any one of the ten proteins in data set by using Gaussian mixture models {Reprinted with permission from Ref. [33]}.

To further avoid protein labelling with fluorophore, a label-free approach for MDS analysis of protein is developed through direct detection of the intrinsic fluorescence of proteins [33,36]. The intrinsic fluorescence of proteins is resulted from aromatic amino acids, such as tyrosine (Tyr) and tryptophan (Trp). Zhang *et al.* [33] reported that the interdiffusion zone with proteins in a MDS device can be directly observed using a home-built UV-LED microscope without any dye-labelling (Fig. 3C) [33]. The R_h of proteins can thus be obtained under their native state in solution. Moreover, by applying emission filters, the fluorescent intensity of Tyr and Trp of a protein can be quantified separately. These multidimensional physical properties of intrinsic fluorescence intensity and hydrodynamic radius show unique fingerprints for protein identification (Fig. 3D).

4.2 Free-flow electrophoresis (FFE)

Apart from the diffusivity and R_h, protein surface charges are also important information for protein analysis [37]. FFE is developed based on diffusional microfluidics to measure protein surface charges by integrating an electric field into diffusional microfluidic devices. Unlike capillary electrophoresis (CE) [38], the electric field is applied perpendicularly to the direction of the flow in FFE devices, molecules travel perpendicular to the electric field [39-40]. The diffusion coefficient of protein can be measured, in theory, using FFE based on the method described above. In addition, electrophoresis measurements in FFE devices enable the calculation of electrophoretic mobility of a protein which can be determined from the electrophoretic velocity and the effective electric field across the electrophoresis channel without the need for reference molecules as mobility standards [41-45]. Consequently, the relative effective charge of a protein can be derived with the measured diffusion coefficient using the equation as below:

$$\mu = \frac{v}{E_{eff}} = \frac{qD}{k_B T}$$

, where μ is electrophoretic mobility, v is electrophoretic drift velocity, E_{eff} is the electric field strength, q is the effective charge, D is diffusion coefficient, k_B is the the Boltzmann constant, T is temperature. Comparing with conventional gel electrophoresis, FFE requires significantly smaller amounts of samples. Moreover, proteins are studied at their native states without the interference of a solid boundary or polymer matrix. Also, joule heat is negligible in a microfluidic device as it can be dissipated efficiently due to the large surface to volume ratios [40-41]. The continuous nature of FFE provides a possibility for high-throughput analysis of proteins [40].

Herling *et al.* [41] designed a FFE device in which the metal electrodes are in direct contact with fluid flow within microfluidic channels. As shown in Fig. 4A, micro-pillar arrays are insert in the FFE device to define the position of the electrodes within the channel, ensuring a homogeneous electric field within

the microchannel. The electric field is applied perpendicularly to the direction of the flow in FFE devices. The flow of analytes occupies the centre of the microchannel and is flanked by streams of buffer. The deflection (δ) upon the application of an electric potential is measured at the end of the microchannel using fluorescence microscopy (Fig. 4A). The electrophoretic velocity, ν, is calculated based on the δ divided by the analyte residence time between the electrodes, which is known from the flow rate through the device and the channel dimensions. E_{eff} across the device is equivalent to V_{eff}/w (w is the width of the channel). Using Ohm's law, the V_{eff} across the solution was determined from the buffer conductance and the measured current. The electrophoretic mobility (μ), thus, is given by the slope of the plots of ν against E_{eff} [41-45]. Therefore, the effective charge of protein can be determined by the obtained electrophoretic mobility (μ) and a given diffusion coefficient (D) of analyte. Using this FFE device, the effective charge of a charge-ladder family of mutant of calcium binding protein calbindin D_{9k} was measured in solution under native conditions [42]. The same authors further [43] investigated the interactions between calmodulin and creatine kinase using the FFE device. The change of electrophoretic mobility of fluorescence labelled calmodulin upon titration of unlabelled creatine kinase was monitored, which proved the formation of the complex of calmodulin and creatine kinase (Fig. 4B).

Moreover, the combination of FFE and MDS can facilitate the charge analysis of unknown protein or protein complex as their diffusion coefficient (D) in solution can be measured by MDS. Zhang *et al.* [45] utilised the same FFE device to characterise the binding equilibrium between aquaporin (AQP0) and calmodulin (CaM) by measuring the changes of electrophoretic mobility of AQP0 as function of CaM concentration under intrinsic protein fluorescence (Fig. 4C). The diffusion coefficient of CaM under different concentration of AQP0 was obtained using a MDS device as described in section 4.1. Therefore, the effective charge of AQP0, CaM and AQP0-CaM complex was determined based on the measured electrophoretic mobility and diffusion coefficient.

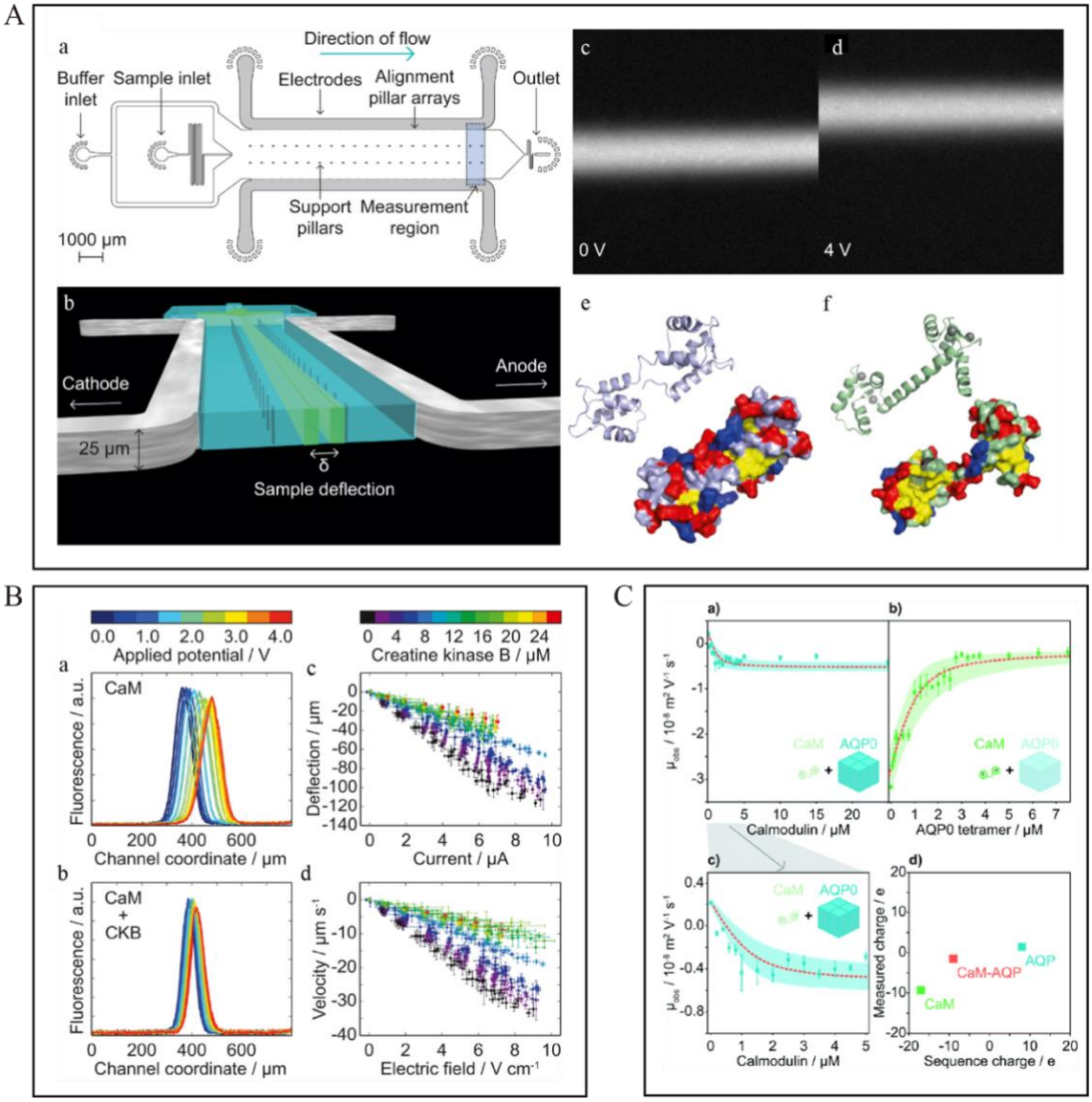

Fig. 4 (A) (a)-(b), The scheme of FFE device. Integrated metal electrodes are shown in gray. Analytes deflect perpendicularly to the flow with applied electric field. The deflection of analytes is detected at the measurement region (measurement region) under fluorescence microscope. (c)-(f), Example of calmodulin 3D structure and its deflection at 0 V and 4 V {Reprinted with permission from Ref. [43]}. (B) Electrophoresis experiment that carried by FFE. (a)-(b), samples (CaM, CaM with CKB) deflection with applied voltage. (c)-(d), the sample deflection against current and sample deflection velocity against the electric field {Reprinted with permission from Ref. [43]}. (C) Investigation of the interactions between membrane protein (AQP0) and calmodulin using FFE by measuring electrophoretic mobility and charge. (a), The changes of electrophoretic mobility of AQP0 as a function of CaM. (b), The changes of electrophoretic mobility of CaM as a function of AQP0 concentration. (c), Expanded view of the data from a. (d), The measured and sequence charges for CaM, AQP0 and CaM-AQP0 {Reprinted with permission from Ref. [45]}.

4.3 Hydrodynamic focusing microfluidic mixer

As mixing at microscale is only contributed by diffusion, T-senser and H-filter allow both temporal and spatial separation of proteins, which enables measurable fluid behaviour of proteins within a microfluidic device. However, it also means that the mixing efficiency within T-sensor and H-filter is low which limits their applications in areas where rapid mixing is required such as study of enzyme kinetics [46] and protein folding [47-48]. Hydrodynamic focusing microfluidic mixer is, thus,

developed based on T-sensors and H-filters to specifically increase the mixing efficiency for protein analysis. It is typically achieved by introducing a middle inlet with analytes in a T-sensor or H-filter to reduce diffusion path and increase the contact surface between fluids [49]. As shown in Fig. 5A and Fig. 5B, the middle stream with analytes can be squeezed to a very small width (as narrow as 50 nm). Reactants from the flanking flows, thus, can diffuse rapidly into the middle flow, leading to rapid mixing. The width of the focusing flow is determined by α.

$$\alpha = \frac{P_s}{P_i}$$

, where P_s is the side flow pressure, and P_i is the middle inlet pressure. By adjusting the flow rate of the middle inlet and the pressure of the flanking flows, the time for solvent mixing within the middle flow can easily obtained below 10 μs [49]. The times scale is critical for studying rapid reaction kinetics which cannot be achieved in a controllable manner by conventional mixing techniques [47-48].

Pollack *et al.* [47] fabricated an x-ray compatible hydrodynamic focusing microfluidic mixer device with rapid mixing channel (Fig. 5C). With this design, the folding steps of the denatured state cytochrome *c* has been studied by time-resolved x-ray scattering. Cytochrome *c* in pH 2 buffer is introduced into the middle inlet and buffer at pH 7 is injected into the side channels, forming a thin section with cytochrome *c*. Solvent molecules from the buffer and the protein flows mix rapidly within the thin section and the pH of the protein flow, thus, increase to above 3 within 200 μs. Comparing to mixing technologies used in previous small-angle x-ray scattering (SAXS) studies, the resolution of mixing time within the hydrodynamic focusing microfluidic mixer device has been increased by almost 2 orders of magnitude, allowing observation of protein folding process triggered by quick pH change. Kratky plot (Fig. 5D) show that the state of denatured cytochrome *c*, at 150 - 500 μs after mixing with buffer solution with high pH, both compact denatured and native states of cytochrome *c* are observed, revealing that cytochrome *c* is one of the fastest folding protein.

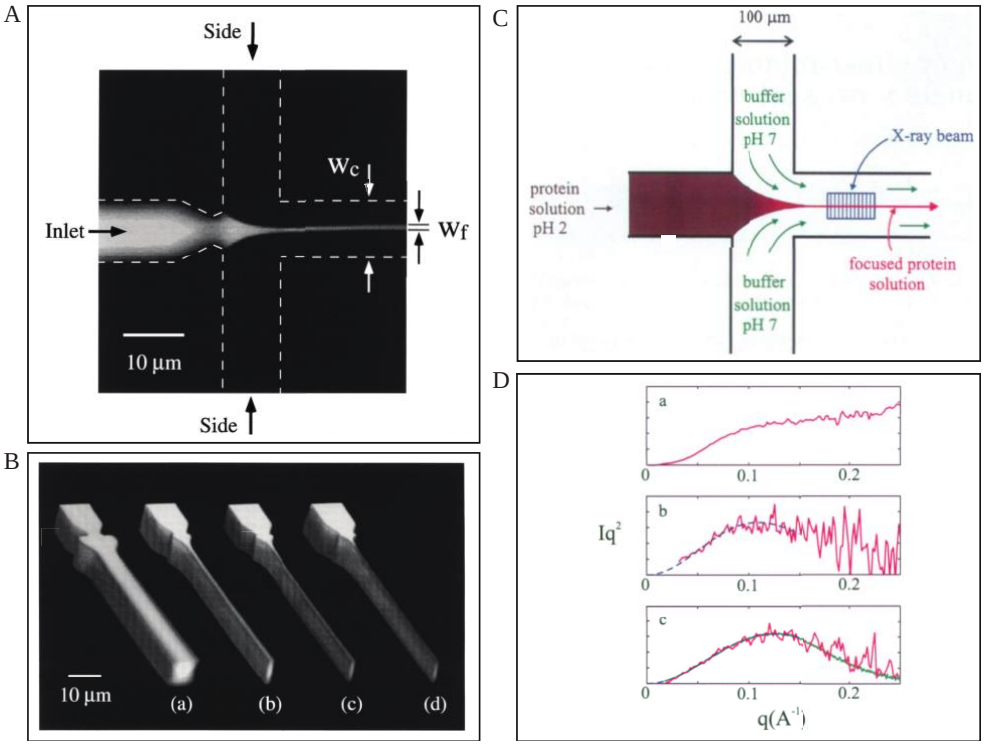

Fig. 5 (A) Hydrodynamic focusing: flow from the inlet channel was labelled by fluorescence dye while non-fluorescence labelled buffer flow from the side channel {Reprinted with permission from Ref. [49]}. (B) Hydrodynamic focusing with $P_i = 5\ psi$ and different values of α with (a) 0.5, (b) 1.0, (c) 1.1, and (d) 1.2 {Reprinted with permission from Ref. [49]}. (C) A schematic of the x-ray compatible hydrodynamic focusing microfluidic mixer {Reprinted with permission from Ref. [47]}. (D) Time-resolved Kratky plots of the data from three different positions in the device. (a) before mixing, (b) after 150 - 500 μs mixing, and (c) after 10 ms mixing time {Reprinted with permission from Ref. [47]}.

5 Conclusion and Perspectives

Diffusional microfluidics, which involve co-flowing streams of analytes and buffer under laminar flow conditions, provides a platform to develop analytical techniques for detection and analysis of analytes such as protein, virus and bacteria. In this review, we have discussed the basis and the working principles of diffusional microfluidics. Three emerging analytical techniques that are based on diffusional microfluidics: microfluidic diffusional sizing (MDS), free-flow electrophoresis (FFE) and hydrodynamic focusing microfluidic mixer are highlighted. In addition, their application in protein analysis is discussed with selected examples which covers protein sizing, protein-protein interaction, protein separation and protein identification. Compared with traditional analytical techniques for protein analysis, such as dynamic light scattering and gel electrophoresis, diffusional microfluidic methods require significantly less samples yet provide higher sensitivity.

Wastewater-based epidemiology (WBE) has been consolidated as an effective tool to monitor public health and the outbreak of infective disease by measuring chemicals, biomarkers and/or pathogenic microorganisms in wastewater generated by people at community-level. To provide real-time information for WBE analysis, it requires analytical techniques that are high-sensitive, cost-efficient and high-throughput to analyse chemicals, biomarkers or pathogens. Thus, MDS, FFE and hydrodynamic focusing microfluidic mixer are promising analytical techniques for WBE. However,

since the three techniques currently mainly focus on protein analysis, one of the important future directions for their application in WBE is to first extend their applications to direct detection and analysis of pathogenic microorganisms and/or other biomarkers such as nucleic acids. In addition, due to the complexity of wastewater in composition, another future direction of MDS, FFE and hydrodynamic focusing microfluidic mixer should focus on development of multifunctional devices that integrate sample purification, detection, analysis and data read-out modules to meet the requirement of analysing the complex wastewater samples.

Declaration of competing interest

The authors declare that they have no known competing financial interests or personal relationships that could have appeared to influence the work reported in this paper.

Acknowledgments

Y. Zhang thanks the Fundamental Research Funds for the Central Universities (lzujbky-2020-45) and the Natural Science Foundation of Gansu Province, China (21JR7RA462).

References

1. Feng, L.Z., Zhang, W. and Li, X.Q., Monitoring of Regional Drug Abuse through Wastewater-Based Epidemiology-a Critical Review. Sci. China Earth Sci., 61(3) (2018) 239-255. https://doi.org/10.1007/s11430-017-9129-x
2. Abdel-Raouf, N., Al-Homaidan, A.A. and Ibraheem, I.B.M., Microalgae and Wastewater Treatment. Saudi J. Biol. Sci., 19(3) (2012) 257-275. https://doi.org/10.1016/j.sjbs.2012.04.005
3. Chahal, C., van den Akker, B., Young, F., Franco, C., Blackbeard, J. and Monis, P., Pathogen and Particle Associations in Wastewater: Significance and Implications for Treatment and Disinfection Processes. Adv. Appl. Microbiol., 97 (2016) 63-119. https://doi.org/10.1016/bs.aambs.2016.08.001
4. Lorenzo, M. and Picó, Y., Wastewater-based epidemiology: current status and future prospects. Curr. Opin. Environ. Sci. Health., 9 (2019) 77-84. https://doi.org/10.1016/j.coesh.2019.05.007
5. Sims, N. and Kasprzyk-Hordern, B., Future Perspectives of Wastewater-Based Epidemiology: Monitoring Infectious Disease Spread and Resistance to the Community Level. Environ. Int., 139 (2020) 105689. https://doi.org/10.1016/j.envint.2020.105689
6. Peccia, J., Zulli, A., Brackney, D.E., Grubaugh, N.D., Kaplan, E.H., Casanovas-Massana, A., Ko, A.I., Malik, A.A., Wang, D., Wang, M.K., Warren, J.L., Weinberger, D.M., Arnold, W. and Omer, S.B., Measurement of Sars-Cov-2 RNA in Wastewater Tracks Community Infection Dynamics. Nat. Biotechnol., 38(10) (2020) 1164-1167. https://doi.org/10.1038/s41587-020-0684-z
7. Barceló, D., Zonja, B. and Ginebreda, A., Toxicity Tests in Wastewater and Drinking Water Treatment Processes: A Complementary Assessment Tool to Be on Your Radar. J. Environ. Chem. Eng., 8(5) (2020) 104262 https://doi.org/10.1016/j.jece.2020.104262
8. Whitesides, G.M.,The Origins and the Future of Microfluidics. Nature, 442(7101) (2006) 368-373. https://doi.org/10.1038/nature05058
9. Jokerst, J.C., Emory, J.M. and Henry, C.S., Advances in microfluidics for environmental analysis. Analyst, 137(1) (2012) 24-34. https://doi.org/10.1039/C1AN15368D
10. Jaywant, S.A. and Arif, K.M., A comprehensive review of microfluidic water quality monitoring sensors. Sensors, 19(21) (2019) 4781. https://doi.org/10.3390/s19214781
11. Song, Y., Lin, B., Tian, T., Xu, X., Wang, W., Ruan, Q., Guo, J., Zhu, Z. and Yang, C., Recent progress in microfluidics-based biosensing. Anal. Chem., 91(1) (2018) 388-404. https://doi.org/10.1021/acs.analchem.8b05007
12. Teh, S.Y., Lin, R., Hung, L.H. and Lee, A.P., Droplet microfluidics. Lab Chip, 8(2) (2008)198-220. https://doi.org/10.1039/B715524G

13. Ou, Y., Cao, S., Zhang, J., Dong, W., Yang, Z. and Yu, Z., Droplet Microfluidics on Analysis of Pathogenic Microbes for Wastewater-Based Epidemiology. TrAC, (2021) 116333. https://doi.org/10.1016/j.trac.2021.116333
14. Squires, T.M. and Quake, S.R., Microfluidics: Fluid physics at the nanoliter scale. Rev. Mod. Phys., 77(3) (2005) 977. https://doi.org/10.1103/RevModPhys.77.977
15. Stone, H.A. and Kim, S., Microfluidics: Basic Issues, Applications, and Challenges. Aiche. J., 47(6) (2001) 1250-1250. https://doi.org/10.1002/aic.690470602
16. Stone, H.A., Stroock, A.D. and Ajdari, A., Engineering Flows in Small Devices: Microfluidics toward a Lab-on-a-Chip. Annu. Rev. Fluid Mech., 36 (2004) 381-411. https://doi.org/10.1146/annurev.fluid.36.050802.122124
17. Brody, J.P., Yager, P., Goldstein, R.E. and Austin, R.H., Biotechnology at Low Reynolds Numbers. Biophys. J., 71(6) (1996) 3430-3441. https://doi.org/10.1016/S0006-3495(96)79538-3
18. Kirby, B.J., Micro-and nanoscale fluid mechanics: transport in microfluidic devices. Cambridge university press. (2010).
19. Müller, T., Arosio, P., Rajah, L., Cohen, S.I.A., Yates, E.V., Vendruscolo, M., Dobson, C.M. and Knowles, T.P.J., Particle-Based Monte-Carlo Simulations of Steady-State Mass Transport at Intermediate Péclet Numbers. Int. J. Nonlinear Sci. Numer. Simul. Int. J. Nonlin. Sci. Num., 17(3-4) (2016) 175-183. https://doi.org/10.1515/ijnsns-2015-0056
20. Kamholz, A.E., Weigl, B.H., Finlayson, B.A. and Yager, P., Quantitative Analysis of Molecular Interaction in a Microfluidic Channel: The T-Sensor. Anal. Chem., 71(23) (1999) 5340-5347. https://doi.org/10.1021/ac990504j
21. Lee, D., Lee, S., Seong, G.H., Choo, J., Lee, E.K., Gweon, D.G. and Lee, S., Quantitative Analysis of Methyl Parathion Pesticides in a Polydimethylsiloxane Microfluidic Channel Using Confocal Surface-Enhanced Raman Spectroscopy. Appl. Spectrosc., 60(4) (2006) 373-377. http://doi.org/10.1366/000370206776593762
22. Lee, S., Choi, J., Chen, L., Park, B., Kyong, J.B., Seong, G.H., Choo, J., Lee, Y., Shin, K.H., Lee, E.K., Joo, S.W. and Lee, K.H., Fast and Sensitive Trace Analysis of Malachite Green Using a Surface-Enhanced Raman Microfluidic Sensor. Anal. Chim. Acta., 590(2) (2007) 139-144. http://doi.org/10.1016/j.aca.2007.03.049
23. Brody, J.P. and Yager, P., Diffusion-Based Extraction in a Microfabricated Device. Sensor Actuat a-Phys, 58(1) (1997) 13-18. https://doi.org/10.1016/S0924-4247(97)80219-1
24. Arter, W.E., Levin, A., Krainer, G. and Knowles, T.P., Microfluidic approaches for the analysis of protein–protein interactions in solution. Biophys. Rev., 12(2) (2020) 575-585. https://doi.org/10.1007/s12551-020-00679-4.
25. Arosio, P., Muller, T., Rajah, L., Yates, E.V., Aprile, F.A., Zhang, Y.B., Cohen, S.I.A., White, D.A., Herling, T.W., De Genst, E.J., Linse, S., Vendruscolo, M., Dobson, C.M. and Knowles, T.P.J., Microfluidic Diffusion Analysis of the Sizes and Interactions of Proteins under Native Solution Conditions. ACS Nano, 10(1) (2016) 333-341. https://doi.org/10.1021/acsnano.5b04713
26. Gang, H., Galvagnion, C., Meisl, G., Muller, T., Pfammatter, M., Buell, A.K., Levin, A., Dobson, C.M., Mu, B.Z. and Knowles, T.P.J., Microfluidic Diffusion Platform for Characterizing the Sizes of Lipid Vesicles and the Thermodynamics of Protein-Lipid Interactions. Anal. Chem., 90(5) (2018) 3284-3290. https://doi.org/10.1021/acs.analchem.7b04820
27. Wright, M.A., Aprile, F.A., Bellaiche, M.M.J., Michaels, T.C.T., Muller, T., Arosio, P., Vendruscolo, M., Dobson, C.M. and Knowles, T.P.J., Cooperative Assembly of Hsp70 Subdomain Clusters. Biochemistry, 57(26) (2018) 3641-3649. https://doi.org/10.1021/acs.biochem.8b00151
28. Scheidt, T., Lapinska, U., Kumita, J.R., Whiten, D.R., Klenerman, D., Wilson, M.R., Cohen, S.I.A., Linse, S., Vendruscolo, M., Dobson, C.M., Knowles, T.P.J. and Arosio, P., Secondary Nucleation and Elongation Occur at Different Sites on Alzheimer's Amyloid-Beta Aggregates. Sci. Adv., 5(4) (2019) eaau3112. http://doi.org/10.1126/sciadv.aau3112
29. Scheidt, T., Carozza, J.A., Kolbe, C.C., Aprile, F.A., Tkachenko, O., Bellaiche, M.M., Meisl, G., Peter, Q.A., Herling, T.W., Ness, S. and Castellana-Cruz, M., The binding of the small heat-shock protein αB-crystallin to fibrils of α-synuclein is driven by entropic forces. PNAS, 118(38) (2021). https://doi.org/10.1073/pnas.2108790118
30. Fiedler, S., Piziorska, M.A., Denninger, V., Morgunov, A.S., Ilsley, A., Malik, A.Y., Schneider, M.M., Devenish, S.R.A., Meisl, G., Kosmoliaptsis, V., Aguzzi, A., Fiegler, H. and Knowles, T.P.J., Antibody Affinity Governs the Inhibition of Sars-Cov-2 Spike/Ace2 Binding in Patient Serum. ACS. Infect. Dis., (2021). https://doi.org/10.1021/acsinfecdis.1c00047
31. Yates, E.V., Muller, T., Rajah, L., De Genst, E.J., Arosio, P., Linse, S., Vendruscolo, M., Dobson, C.M. and Knowles, T.P.J., Latent Analysis of Unmodified Biomolecules and Their Complexes in Solution

with Attomole Detection Sensitivity. Nat. Chem., 7(10) (2015) 802-809. http://doi.org/10.1038/Nchem.2344

32. Bortolini, C., Kartanas, T., Copic, D., Morales, I.C., Zhang, Y., Challa, P.K., Peter, Q., Jávorfi, T., Hussain, R., Dong, M. and Siligardi, G.,.Resolving protein mixtures using microfluidic diffusional sizing combined with synchrotron radiation circular dichroism. Lab Chip, 19(1) (2019) 50-58. https://doi.org/10.1039/C8LC00757H
33. Zhang, Y., Wright, M.A., Saar, K.L., Challa, P., Morgunov, A.S., Peter, Q.A.E., Devenish, S., Dobson, C.M. and Knowles, T.P.J., Machine Learning-Aided Protein Identification from Multidimensional Signatures. Lab Chip (2021). https://doi.org/10.1039/D0LC01148G
34. Ross, J.A. and Jameson, D.M., Time-resolved methods in biophysics. 8. Frequency domain fluorometry: applications to intrinsic protein fluorescence. Photochem. Photobiol. Sci., 7(11) (2008) 1301-1312. https://doi.org/10.1039/B804450N
35. Zhang, Y., Yates, E.V., Hong, L., Saar, K.L., Meisl, G., Dobson, C.M. and Knowles, T.P.J., On-Chip Measurements of Protein Unfolding from Direct Observations of Micron-Scale Diffusion. Chem. Sci., 9(14) (2018) 3503-3507. http://doi.org/10.1039/c7sc04331g
36. Challa, P.K., Peter, Q., Wright, M.A., Zhang, Y.W., Saar, K.L., Carozza, J.A., Benesch, J.L.P. and Knowles, T.P.J., Real-Time Intrinsic Fluorescence Visualization and Sizing of Proteins and Protein Complexes in Microfluidic Devices. Anal. Chem., 90(6) (2018) 3849-3855. http://doi.org/10.1021/acs.analchem.7b04523
37. Lund, M. and Jönsson, B., On the charge regulation of proteins. Biochemistry, 44(15) (2005) 5722-5727. https://doi.org/10.1021/bi047630o
38. Voeten, R.L., Ventouri, I.K., Haselberg, R. and Somsen, G.W., Capillary electrophoresis: trends and recent advances. Anal. Chem., 90(3) (2018) 1464-1481. https://doi.org/10.1021/acs.analchem.8b00015
39. Roman, M.C. and Brown, P.R., Free-flow electrophoresis as a preparative separation technique. Anal. Chem., 66(2) (1994) 86A-94A. https://doi.org/10.1021/ac00074a001
40. Turgeon, R.T. and Bowser, M.T., Micro free-flow electrophoresis: theory and applications. Anal. Bioanal. Chem., 394(1) (2009) 187-198. https://doi.org/10.1007/s00216-009-2656-5
41. Herling, T.W., Muller, T., Rajah, L., Skepper, J.N., Vendruscolo, M. and Knowles, T.P.J., Integration and Characterization of Solid Wall Electrodes in Microfluidic Devices Fabricated in a Single Photolithography Step. Appl. Phys. Lett., 102(18) (2013) 184102. https://doi.org/10.1063/1.4803917
42. Herling, T.W., Arosio, P., Muller, T., Linse, S. and Knowles, T.P.J., A Microfluidic Platform for Quantitative Measurements of Effective Protein Charges and Single Ion Binding in Solution. Phys. Chem. Chem. Phys., 17(18) (2015) 12161-12167. https://doi.org/10.1039/C5CP00746A .
43. Herling, T.W., O'Connell, D.J., Bauer, M.C., Persson, J., Weininger, U., Knowles, T.P. and Linse, S., A Microfluidic Platform for Real-Time Detection and Quantification of Protein-Ligand Interactions. Biophys. J., 110(9) (2016) 1957-1966. https://doi.org/10.1016/j.bpj.2016.03.038.
44. Łapińska, U., Saar, K.L., Yates, E.V., Herling, T.W., Müller, T., Challa, P.K., Dobson, C.M. and Knowles, T.P., Gradient-free determination of isoelectric points of proteins on chip. Phys. Chem. Chem. Phys., 19(34) (2017) 23060-23067. https://doi.org/10.1039/C7CP01503H
45. Zhang, Y., Herling, T.W., Kreida, S., Peter, Q.A.E., Kartanas, T., Tornroth-Horsefield, S., Linse, S. and Knowles, T.P.J., A Microfluidic Strategy for the Detection of Membrane Protein Interactions. Lab Chip, 20(17) (2020) 3230-3238. https://doi.org/10.1039/D0LC00205D
46. Rho, H.S., Hanke, A.T., Ottens, M. and Gardeniers, H., Mapping of enzyme kinetics on a microfluidic device. PloS one, 11(4) (2016) e0153437. https://doi.org/10.1371/journal.pone.0153437
47. Pollack, L., Tate, M.W., Darnton, N.C., Knight, J.B., Gruner, S.M., Eaton, W.A. and Austin, R.H., Compactness of the denatured state of a fast-folding protein measured by submillisecond small-angle x-ray scattering. PNAS, 96(18) (1999)10115-10117. https://doi.org/10.1073/pnas.96.18.10115
48. Hertzog, D.E., Michalet, X., Jäger, M., Kong, X., Santiago, J.G., Weiss, S. and Bakajin, O., Femtomole mixer for microsecond kinetic studies of protein folding. Anal. Chem., 76(24) (2004) 7169-7178. https://doi.org/10.1021/ac048661s
49. Knight, J.B., Vishwanath, A., Brody, J.P. and Austin, R.H., Hydrodynamic focusing on a silicon chip: mixing nanoliters in microseconds. Phys. Rev. Lett., 80(17) (1998) 3863. https://doi.org/10.1103/PhysRevLett.80.3863